Materials Research. 2017; 20(Suppl. 2): 84-91
DOI: http://dx.doi.org/10.1590/1980-5373-MR-2016-0813

LZS/Al_2O_3 Glass-Ceramic Composites Sintered by Fast Firing

Sabrina Arcaro[a,b]*, Maria Isabel Nieto[c], Rodrigo Moreno[c], Maria Dolores Salvador[d], Amparo Borrell[d], Berta Moreno[c], Eva Chinarro[c], Antonio Pedro Novaes de Oliveira[a,b]

[a] *Laboratory of Glass-Ceramic Materials - VITROCER, Federal University of Santa Catarina - UFSC, 88040-900, Florianópolis, SC, Brazil*
[b] *Graduate Program in Materials Science and Engineering - PGMAT, Federal University of Santa Catarina - UFSC, 88040-900, Florianópolis, SC, Brazil*
[c] *Institute of Ceramics & Glass - CSIC, Madrid, Spain.*
[d] *Institute of Materials Technology, Polytechnic University of Valencia, Spain*

Received: October 31, 2016; Revised: March 25, 2017; Accepted: April 9, 2017

In this work, nanometric Al_2O_3 (1-5 vol.%) particles (13 nm, 100 m^2/g) were added to a 19.58Li_2O•11.10ZrO_2•69.32SiO_2 (mol%) (3.5 μm, 2.5 m^2/g) parent glass-ceramic matrix to prepare composites with the purpose of studying the influence of Al_2O_3 on their structure, microstructure, mechanical, thermal and electrical properties when sintered by fast firing. The parent glass-ceramic was prepared by melting and fast cooling (in water) to obtain a glass frit. The resulting glass frit was milled according to a two-step procedure consisting on a dry milling stage followed by a long wet milling step down. Each composition was wet homogenized and then dried at 110 ºC for 48 h for disaggregation. The obtained powders were uniaxially pressed (100 MPa) and compacts sintered by fast firing (175 ºC/min) between 800 and 900 ºC for 30 min. The composites, with relative densities ranging from 89% to 93%, showed zircon and β-spodumene as main crystalline phases. The hardness and Young's modulus varied from 4.5 to 6.5 GPa, and from 65 to 102 GPa, respectively. The formation of β-spodumene in the obtained composites leads to reduce the CTEs, whose values ranged from 13 to 7 x 10^{-6} $ºC^{-1}$.

Keywords: *Alumina nanoparticles, Fast firing sintering, Crystallization, Glass-ceramics*

1. Introduction

The constant advances in the industry require the permanent development of new and efficient solutions for many different applications. In fact, in the last 20 years, the emergence of highly complex structures derived from the junction of several classes of materials. Many efforts have been devoted to improve the mechanical, thermal, electrical and chemical behavior of ceramic materials, exploiting different strategies, such as the study of new compositions, use of reinforcements with particles, fibers, and the use of nanometric secondary phases for ceramic matrix composites and nanocomposites[1-5].

The LZS (Li_2O-ZrO_2-SiO_2) glass-ceramic system has been investigated since 1996[6] due to its interesting properties, particularly from the point of view of its mechanical strength and its hardness and relatively high resistance to abrasion and chemical attack. In fact, relatively recent studies[7,8] have demonstrated that LZS glass-ceramics containing lithium and zirconium silicates ($Li_2Si_2O_5$ and $ZrSiO_4$) as main crystalline phases achieved hardness of 8 ± 0.5 GPa, bending strength of 190 ± 13 MPa and fracture toughness of 3.65 ± 0.20 MPa.$m^{1/2}$. However, most of the LZS glass-ceramic compositions have a relatively high coefficient of thermal expansion, CTE (8.8 - 10 x 10^{-6} $ºC^{-1}$) which constitutes a limitation in some applications. Thus, the production of such LZS glass-ceramics with their inherent properties but with controlled CTE is of practical interest. Some studies[9-14] have been conducted in order to determine the influence of alumina additions in a LZS glass-ceramic matrix, particularly with the purpose of reducing the CTE.

Materials that have low CTE are being developed for applications requiring rapid temperature changes such as heat exchangers, ceramics for use in household cookers, high performance cutting tools and precision optical instruments as well as burner nozzles. Furthermore, in applications involving the joining of materials, the thermal expansion requires a fairly narrow compatibility to match the shrinkage, as in glass and glass-ceramic/metal systems for hermetic seals, laser tubes, electronic devices for measuring and monitoring, sealants for solid oxide fuel cells (SOFCs), and substrates used in microelectronic packaging on LTCC technology (low temperature co-fired ceramics)[15-19].

In previous works[20,21] it was demonstrated that the addition of nanosized alumina in a LZS glass-ceramic matrix, produced by conventional sintering, was able to reduce the CTE significantly. This happens because of the

* e-mail: sabrinarcaro@yahoo.com.br

alumina affinity with respect to lithium silicates to form β-spodumene ($LiAlSi_2O_6$), a crystalline phase having a CTE nearly zero (0.9 x 10^{-6} ºC^{-1}). In this case, the CTE changed from 9.5 x 10^{-6} ºC^{-1} for the LZS glass-ceramic to 4.4 x 10^{-6} ºC^{-1} for a 5 vol.% nanoparticulate alumina LZS glass-ceramic matrix composite.

In this context, this study aims to evaluate the possibility of designing and obtaining of LZS glass-ceramic composites with different nanometric alumina contents sintered and crystallized by fast firing with the aim of generating thermal energy in the furnace at high speed and transmit it to the pieces surfaces to obtain a product of acceptable quality and economically viable. Thus, the influence of the nanometric alumina additions on the structure, microstructure, mechanical and electrical properties and coefficient of thermal expansion, will be evaluated.

2. Experimental Procedure

In this work the following raw materials were used: a LZS glass (parent glass-ceramic powder) with an average particle size $d_{v.50}$=3.5 µm, composition 19.58Li_2O·11.10ZrO_2·69.32SiO_2 (mol%), and a commercially available Al_2O_3 nanopowder (Aeroxide® AluC, Evonik-Degussa, Germany) with an average particle size $d_{v.50}$=13 nm, a specific surface area of 100 m^2/g and made up of a mixture of δ/γ-alumina phase.

Batches to produce the parent glass were prepared from well-mixed powders containing appropriate amounts of Li_2CO_3 (Synth, purity 99%), $ZrSiO_4$ (Colorminas, purity 99%) and SiO_2 (Colorminas, purity 99%) as raw materials. Subsequently, each batch was placed in a Pt crucible (100 mL) and melted at 1550 ºC for 2 h in a high temperature bottom loading furnace (Jung, CPM45, Brazil). The melts were cast into deionized water to provide frits for milling. The resulting glass frit was milled according to a two-step procedure consisting on a dry milling stage followed by a long wet milling step down to an average particle size of $d_{v'50}$=3.5 µm and surface area of 2.5 m^2/g. More details of the milling procedure are available elsewhere[21].

The chemical composition of the milled powder (LZS parent glass) was determined by X-ray fluorescence (Philips, PW 2400, The Netherlands) and atomic absorption spectroscopy (Unican, 969, United Kingdom). Further details on the preparation and processing of the LZS frit are reported in a previous work[20,21].

The differently prepared compositions were labeled as LZS, 1An, 2.5An, and 5An, for contents of nanosized alumina of 0, 1, 2.5, and 5 vol.%. Each composition was wet homogenized (using a water to powder weight ratio of 60/40) on a propeller mechanical agitator (IKA RW Digital 200, Germany). Subsequently, the suspensions of the formulated compositions were dried at 110 ºC for 48 h and then disaggregated into a fast laboratory ball mill (SERVITECH, CT-242, Brazil) for 15 min. Thus, samples of these compositions were uniaxially pressed in a cylindrical steel die by means of a hydraulic press (ST Bovenau P10, Brazil) at 100 MPa. The obtained samples (10 x 6mm) were fired (for sintering and crystallization) in a Bottom Loading Furnace (Energon S.L., Spain) with a heating rate of 175 ºC/min (named fast firing), at 800 and 900 ºC for 30 min. The samples were then immediately taken off and cooled to room temperature with cold air. The firing temperatures were selected based on previous work[20,21]. These works use traditional burning processes. In this new work, the objective is to verify how these composites behave when burned by a rapid burning process. The true densities (ρ_t) of powdered samples were determined by using a helium pycnometer (AccuPyc 1340, Micromeritics, USA). The apparent densities (ρ_a) of fired samples were determined by relating their geometrical measurements, obtained using a caliper (Mitutoyo, Japan, accuracy ± 0.01 mm), and their masses (Shimadzu AX200, Japan, at 0.001 g). The relative densities (ρ_r) were determined relating the apparent densities and the true densities of the samples according to Equation 1.

$$\rho_r = [(\rho_a / \rho_t) \times 100] \quad (1)$$

To determine the evolution of crystalline phases in studied samples, X ray diffraction was performed using a powder XRD (Philips, model X'Pert, The Netherlands) diffractometer using Ni-filtered Cu-Kα radiation (1.5418 Å) at 40 kV and 30 mA. Samples of the composites were rotated to minimize the effect of preferential orientation and analyzed in powder form with particle size smaller than 45 µm, using a step size of 0.02, dwell time of 2 s per step and 2θ between 5 and 80º 2θ angle range. JCPDS data banks were used for identification of the resulting crystalline phases. The quantitative analysis of the crystalline phases has been performed by the Rietveld method[22,23]. The refinement of the X-ray patterns as well as the simulation and quantification of the crystalline phases were performed by the X'Pert HighScore Plus® software (Philips, The Netherlands).

The microstructure of the fired samples was observed on fracture surfaces using a field emission gun scanning electron microscope (FE-SEM-S-4700 type I, Hitachi, Japan). Pore size of the composites were determined from counting corresponding to the specified pore diameters range, based on the linear intercept method[24], where the ratio between the average length string (t) and average sphere diameter (D) is given by Equation 1 to better represent the measurement of a 3D unit (pore) by an 2D image.

$$D = 1.623\, t \quad (2)$$

In this case, five images of the fracture surfaces of obtained were used and 200 measurements in each image (in average) were made, with aid of a software (ImageJ®).

Mechanical properties were evaluated by micro and nanoindentation techniques. Hardness (H) and Young's modulus (E) were measured with a nanoindenter G-200 of

Agilent Technol. (Inc., Santa Clara, CA) under a 2000 nm constant indentation depth program. A Berkovich tip was used after calibration of the function area in fused silica sample. Stiffness was recorded in depth by Continuous Stiffness Measurement (CSM). The oscillation amplitude was programmed to 2 nm with a frequency of 45 Hz. Sixteen indentations with 100 μm spacing between them were arranged in a matrix (4 x 4) for all samples analyzed.

Two-point probe electrical conductivity measurements have been performed in the thermal treated samples (disks with 6.5 mm in diameter). The electrical contact was made by sandwiching the disk shaped samples with Pt foils using coils to ensure good contacts. The sandwiched sample was inserted into the furnace and the electrical resistance was measured in the range of 300-900 ºC in air atmosphere by impedance measurements in the range of 1 MHz - 10 Hz (Agilent 4294A) with an amplitude of 50 mV. It is noteworthy that for temperatures below 300 ºC it has not been possible to obtain the impedance curve with precision, because the electrical conductivity is very low in relation to the effects of the electrode.

The acquired impedance spectra were analyzed using the ZVIEW® fitting software. The activation energy and electrical conductivity at room temperature were obtained from an Arrhenius plot[25,26]. According to the Arrhenius equation the relation between ionic conductivity in solids and the temperature T is given by Equation 2:

$$\ln(\sigma.T) = \frac{-EA}{kT} \quad (3)$$

where EA is the activation energy for the electrical conduction processes[26].

The coefficient of thermal expansion (CTE) of the composites was measured linearly from the thermal expansion curve, and was determined using a contact dilatometer (Netzsch Gerätebau model 402 EP, Germany) at a heating rate of 5 ºC/min in the temperature range between 25 and 500 ºC.

3. Results and Discussion

Table 1 shows the theoretical chemical composition and experimental values obtained by chemical analysis of the LZS parent glass powder.

As can be seen, there is a small difference between the theoretical chemical composition and experimental values obtained by chemical analysis of the LZS parent glass powder. In fact, there is a small decrease in the percentage related to the lithium oxide, probably due to some evaporation of Li during melting. The detection of aluminum oxide can be associated to the contamination produced by the wear of the alumina balls used for milling. In spite of this alumina contamination it, apparently, did not affect the expected performance of the obtained LZS glass-ceramics.

Table 2 shows the relative density for LZS glass-ceramic samples (without Al_2O_3) and for the composites containing 1, 2.5 and 5 vol.% of nanosized Al_2O_3 fired by fast firing at 800 ºC and 900 ºC for 30 min. It can be seen that the relative densities of the samples are between 89 and ~ 93 %. From the data collected one can realizes that for the two studied fast firing temperatures, the relative density of the sintered samples slight decreases with increasing amount of added alumina, but less than it could be expected. This behavior can be explained due to the presence of nanosized alumina which is more reactive than the LZS glass matrix, reducing the viscous flow during sintering step, and retarding densification. This retard is related to the crystallisation of spodumene crystalline phase, which greatly reduces the sintering rate. Viscous flow reduction may in this case be by mechanical impediment (thermal stability of the alumina) and/or by dissolution of the latter in the glass forming crystalline phases (such as lithium aluminum silicates) more viscous. In fact, some works in the literature[27,28] support these possibilities since there is a decrease in the relative density of glass samples containing different amounts of alumina particles. It is also verified that the effect intensifies as the particle size decreases[27]. In this context, according to[28] a strong coupling between alkali ions in borosilicate glass and Al^{+3} in alumina, forms an Al^{+3} and alkali ion-rich reaction layer around alumina particles. Since the above reaction continuously depletes the concentration of alkali ions in the glass during sintering, it causes a rise in viscosity of the glass and thus slows down the densification kinetics and increases the activation energy of densification.

Table 1. Chemical composition of the LZS parent glass.

Constituent oxides	Composition (wt%)	
	Theoretical[6]	Analyzed
Al_2O_3	---	0.95
CaO	---	0.05
Fe_2O_3	---	0.05
Li_2O	9.6	8.63
Na_2O	---	0.05
SiO_2	68.1	68.02
TiO_2	---	0.05
ZrO_2	22.4	22.20

Table 2. Relative densities of samples sintered at 800 ºC and 900 ºC for 30 min.

Compositions	Sintered density (%TD)	
	800 ºC	900 ºC
LZS GLASS-CERAMIC	93 ± 0.2	94 ± 0.5
LZS-1An	90 ± 0.5	92 ± 0.5
LZS-2.5An	90 ± 0.5	93 ± 0.5
LZS-5An	89 ± 0.5	90 ± 0.5

Table 2 shows that the relative densities of samples fired (sintered) at 900 ºC are slightly higher than those of samples fired at 800 ºC for 30 min. This behavior can be related to the differences in the resulting microstructures for composites fired by fast firing at 800 ºC (a) and 900 ºC (b) as shown in Figure 1.

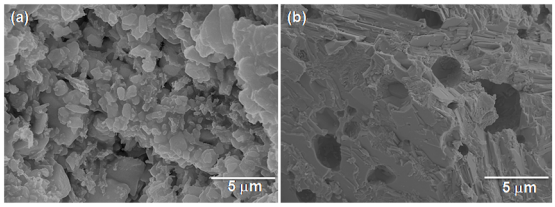

Figure 1. SEM micrographs of fracture surfaces of fast fired LZS. (a) 800 ºC, and (b) 900 ºC for 30 min.

It can be seen by analysis of Figure 1 that samples fired at 800 ºC did not readily sinter to high density. At 900 ºC, the particles form a single homogeneous body, although some porosity is still remaining, which was expected for such glass-ceramics produced from powders in accordance with the obtained density measurements. The microstructural difference enables the selection of composites with enhanced performance for further evaluation of the behavioral properties. Thus, selected composites were sintered by fast firing at 900 ºC. Figure 2 shows SEM micrographs of fracture surfaces of the LZS glass-ceramic (a) without and with different alumina additions after fast firing at 900 ºC for 30 min (b, c, d).

The micrographs confirm the information obtained from the relative density versus firing temperature curves, i.e., the porosity is very similar in all cases, although there is a small increase as the alumina content increases from 1% to 5%. However, it must be noted that the pore size decreases with increasing amount of alumina added to the LZS glass-ceramic. Figures (e) and (f) are at higher magnification to better demonstrate pore sizes. It was possible to calculate the mean pore diameter size from the measurements performed by the intercept method. For the LZS sample an average value of 3.50 ± 0.5 µm was obtained. For the 5An sample, a value of 2.75 ± 0.6 µm was obtained.

Figure 3 shows the obtained X-ray diffraction patterns of the LZS parent glass (a), LZS glass-ceramic sintered by fast fired at 800ºC (b), LZS glass-ceramic sintered by fast fired at 900 ºC (c) and LZS with different alumina additions (d, e, and f) fast fired at 900 ºC for 30 min. The X-ray diffractogram shown in Figure 3 (a), exhibits a band at about 23º which is characteristic of amorphous phase, i.e., the LZS parent glass-ceramic. In addition, it is possible to observe that the crystallization phenomenon practically did not happen for the LZS glass ceramic sintered at 800 ºC by fast firing, i.e. it is possible to observe the band at about 23º. This fact, as well the density and microstructure, supported in the selection of the samples at 900 º C for further work. It was verified from the data collected from the XRD patterns related to the LZS glass-ceramic (c) that zirconium silicate, $ZrSiO_4$, lithium disilicate, $Li_2Si_2O_5$ and β-quartz are the crystalline phases formed. It is observed also that the addition of Al_2O_3 (d, e, and f) promotes the formation of β-spodumene, $LiAlSi_2O_6$ and lithium metasilicate, Li_2SiO_3 phases.

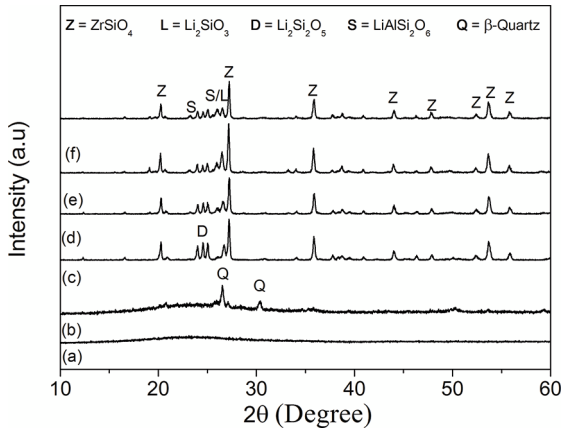

Figure 3. X-ray diffraction patterns of the LZS parent glass (a), LZS glass-ceramic sintered by fast fired at 800 ºC (b), LZS glass-ceramic sintered by fast fired at 900 ºC (c), and LZS with different alumina additions (c, d, and e) fast fired at 900 ºC/30 min. (Z) zirconium silicate, $ZrSiO_4$; (D) lithium disilicate, $Li_2Si_2O_5$; (Q) β-quartz; (S) β-spodumene, $LiAlSi_2O_6$ and (L) lithium metasilicate, Li_2SiO_3.

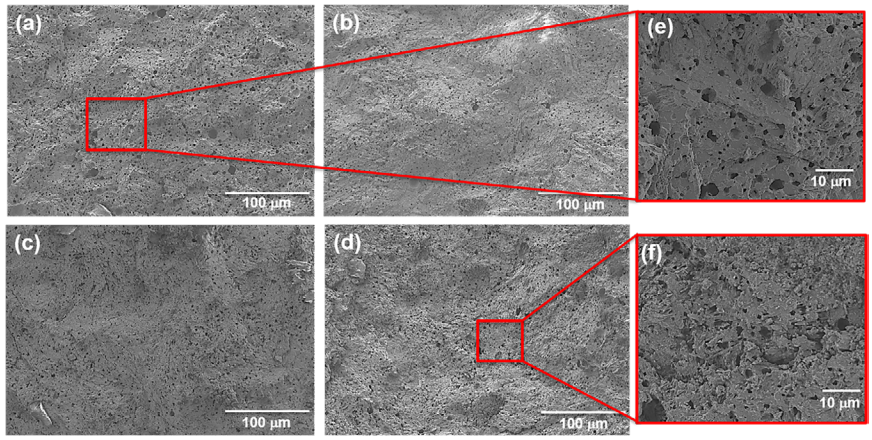

Figure 2. SEM micrographs of fracture surfaces of the LZS glass-ceramic without (a), with 1, 2.5, and 5 vol.% (b, c, and d, respectively) alumina additions after fast firing at 900 ºC for 30 min and LZS glass-ceramic (e) and LZS with 5 vol% alumina additions (f) for a high magnification.

Table 3 shows the relative amounts of crystalline phases determined by Rietveld refinement of the LZS glass-ceramic samples (without Al_2O_3) and of the LZS/nano Al_2O_3 composites containing 1, 2.5 and 5 vol.% of nanosized Al_2O_3 fast fired at 900 ºC for 30 min. It can be noticed that the LZS glass-ceramic has 35.8% of zirconium silicate, 44.7% of lithium disilicate and 19.5% of β-quartz. Note that when adding alumina in the LZS glass-ceramic composition, there is a gradual decrease of lithium disilicate and the formation of β-spodumene phase, so that lithium metasilicate formation is promoted. This is due to the presence of alumina, which has high affinity for lithium and they easily react to form β-spodumene. Since the molar ratio between alumina and lithium is not stoichiometric the β-spodumene phase is accomplished by the formation of lithium disilicate and lithium metasilicate. For the composition containing only 1 vol.% of Al_2O_3, the formation of β-spodumene determinated by Rietveld method to occur to an extent of 16.1%. For compositions containing 2.5 and 5 vol.% nano alumina, the determined β-spodumene contents are 19.3 and 28.4%. This crystalline phase is very interesting from the point of view of properties that can enhance the glass-ceramic behavior, mainly due to its low coefficient of thermal expansion[12-14,29]. No crystalline phases based on alumina could be detected by XRD.

Table 4 shows the values of Vickers microhardness and Young's modulus, for LZS glass-ceramic samples (without Al_2O_3) and for the composites containing 1, 2.5 and 5 vol.% of nanosized Al_2O_3 fired by fast firing at 800 ºC and 900 ºC for 30 min. It can be seen that both values of microhardness and Young's modulus for composites sintered at 900 ºC are higher than those for samples sintered at 800 ºC, as expected. According to that seen in Figure 1, the later has a high porosity, open microstructure and heterogeneous particles that still retain their identity, thus explaining the lower values of hardness and Young modulus. However, good results of Vickers microhardness were obtained for samples fired at 900 ºC for 30 min with values ranging from 4.9 to 6.5 GPa. These good results can be associated with the presence of zirconium silicate crystals which have hardness between 9 and 10 GPa[24]. It is possible to observe that there was a slight decrease in Vickers microhardness values with the addition of Al_2O_3. This fact can be explained for although the amount of the β-spodumene crystalline phase which has a hardness value lower than that of zircon[29-31]. Furthermore, considering the increase of porosity with an increase of the addition Al_2O_3, is possible residual porosity exerts a negative influence on the mechanical properties of the sintered ceramics[32-34].

Table 4. Mechanical properties of samples fast fired at 800 and 900 ºC for 30 min.

Compositions	Mechanicalproperties			
	Vickers Microhardness, HV (GPa)		Young's Modulus, E (GPa)	
	800 ºC	900ºC	800ºC	900ºC
LZS GLASS-CERAMIC	6 ± 0.3	6.5 ± 0.4	92 ± 0.5	102 ± 0.5
LZS-1AN	5.7 ± 0.4	6.4 ± 0.4	90 ± 0.5	98 ± 0.5
LZS-2.5AN	5.7 ± 0.4	5.0 ± 0.2	90 ± 0.4	79 ± 0.3
LZS-5AN	4.3 ± 0.2	4.9 ± 0.1	65 ± 0.3	72 ± 0.2

The Young's modulus (E), have a fluctuation with a slight decrease with increasing amount of added alumina ranging from 102 GPa to 72 GPa for the LZS composition without and with 5% Al_2O_3, respectively. This fact could be associated mainly with the increased porosity with the addition of alumina since it is well known that the Young's modulus decreases exponentially with the porosity[32-34].

The electrical conductivity as a function of the temperature was investigated using two-point probe measurement, getting the resistance (Z '= R when Z' = 0 in the impedance diagram, the side of low frequencies), with the aid of Zview® software so that an Arrhenius plot (Figure 4) can be drawn from which the activation energy for the conduction process can be calculated.

Table 3. Relative amounts of crystalline phases(Rietveld refinement)for samples of the LZS glass-ceramic without and with different alumina additions fired by fast fired at 900 ºC/30 min.

Crystalline phase	Chemical formula	Relative amounts of crystalline phases (wt%)			
		LZS glass-ceramic	LZS -1An	LZS - 2.5An	LZS - 5An
Zirconium silicate (ICSD 100248)	ZrSiO4	35.8	31.5	30.8	29.5
Lithium disilicate (ICSD 15414)	$Li_2Si_2O_5$	44.7	31.5	20.4	15
β-Quartz (ICSD 64980)	SiO_2	19.5	16.6	19.7	13.4
β-spodumene (ICSD 14235)	$LiAlSi_2O_6$	-	16.1	19.3	28.4
Lithium metasilicate (ICSD 28192)	Li_2SiO_3	-	4.3	9.9	13.7
GOF: Godnness of fit		1.84	1.73	1.48	1.87

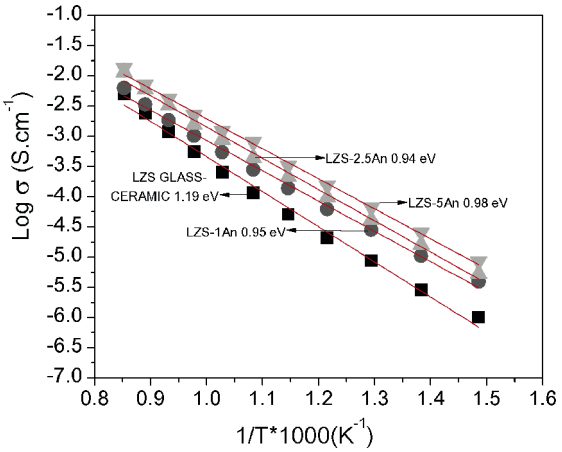

Figure 4. Arrhenius plot (Log conductivity versus the inverse of temperature) for samples of the LZS glass-ceramic (without Al_2O_3) and for the composites containing 1, 2.5 and 5 vol.% of nanosized Al_2O_3 sintered by fast firing at 900 ºC for 30 min.

In all composites the electrical conductivity increases with temperature showing a semiconductor behaviour, from values around 10^{-6} S.cm^{-1} at 300 ºC to values around 10^{-2} S.cm^{-1}at 900 ºC, as it could be expected. In general, the Arrhenius plots indicate that for the whole temperature range tested the electrical conductivity remains higher with the addition of alumina. This fact is in opposition to the expected behavior, since alumina is an insulating material, as for example the values measured at low temperatures, in this case 300 ºC, the conductivity obtained is about 8 orders of magnitude higher that expected for alumina and silica, which exhibits conductivities around 10^{-14} S.cm^{-1} at this temperature. But the conduction process of these materials is heavily influenced by the concentration of Li ions that have high mobility, exhibiting ionic conductivities as reported in the literature[26,29,31,35].

The activation energy for all cases decreased with increasing addition of alumina. This fact is probably related to the presence of increasing contents of β-spodumene phase with larger additions of alumina. Other authors have reported that glass-ceramics containing this phase have electrical conductivity values in the same range[26,29].

It can be observed as the conductivity as the CTE are directly related to the phases crystalized when Al_2O_3 is added, $LiAlSi_2O_6$ and Li_2SiO_3. The conductivity and thermal expansion coefficient are influenced by the materials partners of the matrix. Conductivity is higher when Al_2O_3 because three Li-materials exhibit high lithium mobility, even Li_2SiO_3 does not appear to be a particularly good ionic conductor, it is still likely that the local mechanism of Li+ site exchange is similar to that in better-studied silicates[36]. Also, the CTE of a glass-ceramic material depends on the single CTEs of its crystalline and amorphous phases and their proportions[37-39] and at this respect, the lower CTE of $LiAlSi_2O_6$ than $Li_2Si_2O_5$ is doing to decrease the CTE of LZS/Al_2O_3 sintered in this work.

To complete the characterization of LZS-Al_2O_3 composites obtained by fast firing the coefficients of thermal expansion were determined. According to the results shown in Figure 5, the coefficients of thermal expansion (CTE) decrease gradually with the amount of alumina added from 11.3 x 10^{-6} ºC^{-1} for the LZS glass-ceramic (fast fired at 900 ºC for 30 min) to 6.0 x 10^{-6} ºC^{-1} for the composition LZS-5An. This significant CTE decrease with increasing amount of added alumina is related to a fraction of transformed zirconium silicate (which has a relatively low CTE, i.e., 4 x 10^{-6} ºC^{-1}) and in particular to the formation of the β-spodumene phase (which has a much lower CTE, i.e., 0.4-2 x 10^{-6} ºC^{-1}) as reported in the XRD patterns of Figure 3.

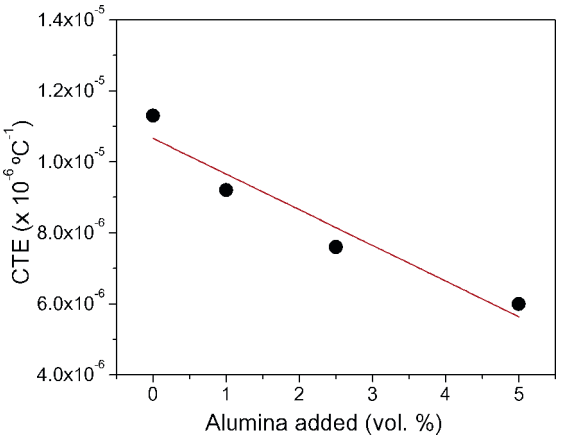

Figure 5. Coefficients of thermal expansion for the LZS glass-ceramic (without Al_2O_3) and for the LZS + Al_2O_3 composites containing 1, 2.5 and 5 vol.% of nanosized Al_2O_3 fast fired at 900 ºC for 30 min.

4. Conclusions

LZS-Al_2O_3 composites with glass-ceramic matrix $19.58Li_2O.11.10ZrO_2.69.32SiO_2$ (3.5 μm) and nanoparticles (13 nm) of Al_2O_3 (1-5 vol.%) were prepared by melting of a LZS parent glass and further mixing and reaction in the solid state with Al_2O_3 nanoparticles. The obtained composites were sintered by fast firing at 800 and 900 ºC for 30 min, leading to relative densities between 89 and 94%, containing zirconium silicate and β-spodumene as major crystalline phases. Composites sintered by fast firing at 900 ºC, had hardness between 4.5 and 6.5 GPa and Young's modulus between 65 and 102 GPa, the highest value being achieved for the LZS glass-ceramic. The electrical conductivity was maintained within ± 10^{-6} S.cm^{-1}. The formation of β-spodumene in the obtained composites leads to reduce the CTE, whose values ranged from 11.3 to 6 x 10^{-6} ºC^{-1}.

5. Acknowledgments

This work has been supported by CAPES in the frame of the International Cooperation Program Science without Borders for Special Visiting Researcher PVE (MEC/MCTI/CAPES/CNPq/FAPESC/Nº71/2013), Project Nº A011/2013 (Brazil)

and CNPq (National Council for Scientific and Technological Development, Brazil). Authors greatly acknowledge the financial Support of the Spanish Ministry of Economy and Competitiveness (MINECO, grant MAT2015-67586-C3-R, ENE2013-49111-C2-1-R, and IJCI-2014-19839).

6. References

1. Rajan VP, Zok FW. Matrix cracking of fiber-reinforced ceramic composites in shear. *Journal of the Mechanics and Physics of Solids*. 2014;73:3-21.

2. Wei J, Pećanac G, Malzbender J. Mechanical behavior of silver reinforced glass-ceramic sealants for solid oxide fuel cells. *Ceramics International*. 2015;41(10 Pt B):15122-15127.

3. Widjaja S. Determination of creep-induced residual stress in fiber-reinforced glass-ceramic matrix composites by X-ray diffraction. *Materials Characterization*. 2001;47(1):47-54.

4. Camargo PHC, Satyanarayana KG, Wypych F. Nanocomposites: synthesis, structure, properties and new application opportunities. *Materials Research*. 2009;12(1):1-39.

5. Xia L, Jin F, Zhang T, Hu X, Wu S, Wen, G. Enhanced oxidation resistance of carbon fiber reinforced lithium aluminosilicate composites by boron doping. *Corrosion Science*. 2015;99:240-248.

6. Oliveira APN, Barbieri L, Leonelli C, Manfredini T, Pellacani GC. Physical Properties of Quenched Glasses in the Li_2O-ZrO_2-SiO_2 System. *Journal of the American Ceramic Society*. 1996;79(4):1092-1094.

7. Teixeira JD, Oliveira APN, Bohels L, Cesconeto FR, Siligardi C, Pereira MA. Sintering Behaviour of LZS Glass-Ceramics. *Materials Science Forum*. 2012;727-728;1028-1033.

8. Domingos Teixeira J, Pereira MA, Boehs L, Siligardi C, Cantavella V, Oliveira APN. Physical-Mechanical Behaviour of a LZS Glass-Ceramic. *Materials Science Forum*. 2014;775-776:599-603.

9. Arcaro S, Cesconeto FR, Raupp-Pereira F, Oliveira APN. Synthesis and characterization of LZS/α-Al_2O_3 glass-ceramic composites for applications in the LTCC technology. *Ceramics International*. 2014;40(4):5269-5274.

10. Gomes C, Travitzky N, Greil P, Acchar W, Birol H, Oliveira APN, et al. Laminated object manufacturing of LZSA glass-ceramics. *Rapid Prototyping Journal*. 2011;17(6):424-428.

11. Oliveira APN, Manfredini T, Pellacani GC, Bonamartini A, Di Landro L. Al_2O_3 Particulate-Reinforced LZS Glass Ceramic Matrix Composites. In: *9th CIMTEC Word Ceramics Congress, Part C*. Vicenzini P, ed. Faenza: Techna Srl; 1999. p. 707-714.

12. Montedo ORK, Floriano FJ, Oliveira Filho J. Sintering kinetics of a $18.8Li_2O.8.3ZrO_2.64.2SiO_2.8.7Al_2O_3$ glass ceramic. *Ceramics International*. 2011;37(6):1865-1871.

13. Montedo ORK, Hotza D, Oliveira APN, Meszaros R, Travitzky N, Greil P. Crystallisation Kinetics of a β-Spodumene-Based Glass Ceramic. *Advances in Materials Science and Engineering*. 2012;2012:525428.

14. Montedo ORK, Bertan FM, Piccoli R, Hotza D, Klein AN, Oliveira APN. Low Thermal Expansion Sintered LZSA Glass-Ceramics. *American Ceramic Society Bulletin*. 2008;87(7):34-40.

15. Benavente R, Salvador MD, García-Moreno O, Peñaranda-Foix FL, Catalá-Civera JM, Borrell A. Microwave, Spark Plasma and Conventional Sintering to Obtain Controlled Thermal Expansion β-Eucryptite Materials. *International Journal of Applied Ceramic Technology*. 2015;12(Suppl 2):E187-E193.

16. Durán A, Pascual L, Pascual MJ. *Vidrios y vitrocerámicos para soldadura: usos tradicionales y nuevas áreas de aplicación*. Boletin de la Sociedad Española de Ceramica y Vidrio. 1995;36:383-398.

17. Smeacetto F, Salvo M, Santarelli M, Leone P, Ortigoza-Villalba GA, Lanzini A, et al. Performance of a glass-ceramic sealant in a SOFC short stack. *International Journal of Hydrogen Energy*. 2013;38(1):588-596.

18. Haydn M, Ortner K, Franco T, Uhlenbruck S, Menzler NH, Stöver D, et al. Multi-layer thin-film electrolytes for metal supported solid oxide fuel cells. *Journal of Power Sources*. 2014;256:52-60.

19. Timurkutluk B, Ciflik Y, Korkmaz H. Strength evaluation of glass-ceramic composites containing yttria stabilized zirconia after thermal cycling. *Ceramics International*. 2015;41(5 Pt B):6985-6990.

20. Arcaro S, Nieto MI, Rodrigues Neto JB, Oliveira APN, Moreno R. Al_2O_3 Nanoparticulate LZS Glass-Ceramic Matrix Composites for Production of Multilayered Materials. *Journal of the American Ceramic Society*. 2016;99(11):3573-3580.

21. Arcaro S, Nieto MI, Moreno R, Oliveira APN. The influence of nano alumina additions on the coefficient of thermal expansion of a LZS glass-ceramic composition. *Ceramics International*. 2016;42(7):8620-8626.

22. Kemethmüller S, Roosen A, Goetz-Neunhoeffer F, Neubauer J. Quantitative Analysis of Crystalline and Amorphous Phases in Glass-Ceramic Composites Like LTCC by the Rietveld Method. *Journal of the American Ceramic Society*. 2006;89(8):2632-2637.

23. Sakata M, Cooper MJ. An analysis of the Rietveld Profile Refinement Method. *Journal of Applied Crystallography*. 1979;12:554-563.

24. ASTM International. *ASTM D 3576 - 98. Standard Test Method for Cell Size in Rigid Cellular Plastics*. West Conshohocken: ASTM International; 1998. 5 p.

25. West AR. *Solid State Chemistry and its Aplications*. 2nd ed. Hoboken: Wiley; 2014. 584 p.

26. West AR. Ionic conductivity of oxides based on Li_4SiO_4. *Journal of Applied Electrochemistry*. 1973;3(4):327-335.

27. Araújo PF, Daros LB, Souza M, García DE, Hotza D. Influence of Sintering Conditions on the Microstructure and Properties of Alumina-Filled Borosilicate Glass. *Journal of Ceramic Science and Technology*. 2016;7(1):119-126.

28. Jean JH, Gupta TK. Effect of alumina on densification of binary borosilicate glass composite. *Journal of Materials Research*. 1994;9(8):1990-1996.

29. Nuernberg RB, Faller CA, Montedo ORK. Crystallization kinetic and thermal and electrical properties of β-spodumene$_{ss}$/cordierite glass-ceramics. *Journal of Thermal Analysis and Calorimetry*. 2017;127(1):355-362.

30. Shi Y, Huang X, Yan D. Fabrication of hot-pressed zircon ceramics: Mechanical properties and microstructure. *Ceramics International*. 1997;23(5):457-462.

31. Montedo ORK, Alves IT, Faller CA, Bertan FM, Piva DH, Piva RH. Evaluation of electrical properties of glass-ceramics obtained from mill scale. *Materials Research Bulletin*. 2015;72:90-97.

32. Awaad M, Mörtel H, Naga SM. Densification, mechanical and microstructure properties of β-spodumene-alumina composites. *Journal of Materials Science: Materials in Electronics*. 2005;16(6):377-381.

33. Benavente R, Salvador MD, Martínez-Amesti A, Fernández A, Borrell, A. Effect of sintering technology in β-eucryptite ceramics: Influence on fatigue life and effect of microcracks. *Materials Science and Engineering: A*. 2016;651:668-674.

34. Thompson JY, Stoner BR, Piascik JR. Ceramics for restorative dentistry: Critical aspects for fracture and fatigue resistance. *Materials Science and Engineering: C*. 2007;27(3):565-569.

35. Winter R, Siegmund K, Heitjans P. Nuclear magnetic and conductivity relaxations by Li diffusion in glassy and crystalline $LiAlSi_4O_{10}$. *Journal of Non-Crystalline Solids*. 1997;212(2-3):215-224.

36. George AM, Richet P, Stebbins JF. Cation dynamics and premelting in lithium metasilicate (Li_2SiO_3) and sodium metasilicate (Na_2SiO_3): A high-temperature NMR study. *American Mineralogist*. 1998;83:1277-1284.

37. Rampf M, Fisch M, Dittmer M, Ritzberger C, Schweiger M, Höland W. Tailoring the Thermal Expansion of Glass-Ceramics by Controlled Twofold Crystallization of $Li_2Si_2O_5$ and $CsAlSi_5O_{12}$. *International Journal of Applied Glass Science*. 2016;7(3):285-294.

38. Höland W, Beall GH. *Glass-Ceramic Technology*. 2nd ed. Hoboken: Wiley; 2012. 440 p.

39. Loehman RE, Headly TJ. Design of High Thermal Expansion Glass-Ceramics Through Microstructural Control. In: Pask JA, Evans EG. *Ceramic Estructures '86 - Role of Interfaces*. New York: Plenum Press; 1987. p. 33-43.